

TESTING OF A REPAIRED MICRO-CONCRETE
MODEL OF A COOLING TOWER SHELL

by

HOSSEIN MOZAFFARIAN

B.S., Kansas State University, 1980

A MASTER'S THESIS

submitted in partial fulfillment of
the requirements for the degree

MASTER OF SCIENCE


Department of Civil Engineering

KANSAS STATE UNIVERSITY

Manhattan, Kansas

1983

Approved by

A handwritten signature in cursive script, appearing to read "Stuart Edwards", is written over a horizontal dashed line.

Major Professor

LD
2668
.T4
1983
M69
C.2

111202 570989

Table of Contents

	Page
List of Tables	ii
List of Figures	iii
Synopsis	1
Chapter I. Introduction	3
Chapter II. Review of Literature	5
Chapter III. Shell Test Arrangements	12
Strain and Displacement Instrumentation ...	12
Loading Equipment and Testing Procedure ...	13
Chapter IV. Test Results and Analysis	15
Shell Geometry	15
Shell Thickness	16
Structural Response and Failure	17
Chapter V. Conclusions	27
Appendix A. Tables	29
Appendix B. Figures	40
Appendix C. Sample Calculations	90
Appendix D. Notation	99
Acknowledgements	102
List of References	103
Abstract	

List of Tables

Table	Page
1. Properties of the Patching Mix, Steel Reinforcing, and Support Column	30
2. Cylinder Test Results, Shell No.1	31
3. Original Surface Deviation from Ideal Geometry, Shell No.1	32
4. Shell Thickness, Shell No.1	33
5. Improved Data of Deviation From Ideal Mid-Surface Geometry Considering Actual Thicknesses, Shell No.1.	34
6. Percent Deviation From Mean Thickness for Lifts 2 and 3 of Shell No. 1	35
7. Percent Deviation From Mean Thickness for Mungan's Plastic Models (26)	36
8. Experimental Forces and Bending Moments at the Location of Strain Gages at Max. Load of 3.7 Psi, Shell No. 1	37
9. Values of the Coefficients for the Deviation Function, $e = \sum_{n=0}^{\infty} [A_n \cos(n\theta) + B_n \sin(n\theta)]$	38
10. Predicted Pressure Associated with Possible Local Buckling, Shell No. 1	39

List of Figures

Figure	Page
1. Shell Geometry	41
2. Meridional Locations for Thickness, Geometry, Displacement, and Strain Data	42
3. Circumferential Locations for Thickness, Geometry, and Displacement Data, Shell No.1	43
4. Geometrical Representation of Deviation Considering Actual Thicknesses	44
5. Deviation Profile From Ideal Geometry for Level No.1 of Shell No.1	45
6. Deviation Profile From Ideal Geometry for Level No.2 of Shell No.1	46
7. Deviation Profile From Ideal Geometry for Level No.3 of Shell No.1	47
8. Deviation Profile From Ideal Geometry for Level No.4 (Throat) of Shell No.1	48
9. Deviation Profile From Ideal Geometry for Level No.5 of Shell No.1	49
10. Deviation Profile From Ideal Geometry for Level No.6 of Shell No.1	50
11. Deviation Profile From Ideal Geometry for Level No.7 of Shell No.1	51
12. Deviation Profile From Ideal Geometry for Level No.8 of Shell No.1	52

List of Figures (Continued)

Figure	Page
13. Deviation Profile From Ideal Geometry for Level No.9 of Shell No.1	53
14. Deviation Profile From Ideal Geometry for Level No.10 of Shell No.1	54
15. Deviation Profile From Ideal Geometry for Level No.11 of Shell No.1.....	55
16. Thickness Contours, Shell No.1	56
17. Strain Versus Load at Line H, Top of Shell- Just Below Ring Beam (Meridional), Shell No.1, Tested on 19 Feb., 1982	57
18. Strain Versus Load at Line H, Top of Shell- Just Below Ring Beam (Circumferential), Shell No.1, Tested on 19 Feb., 1982	58
19. Strain Versus Load at Throat, Line H, Shell No.1, Tested on 19 Feb., 1982	59
20. Strain Versus Load at Throat, Line E, Shell No.1, Tested on 19 Feb., 1982	60
21. Strain Versus Load at Throat, Line B, Shell No.1, Tested on 19 Feb., 1982	61
22. Strain Versus Load at Four Feet Below Throat, Line H, Shell No.1, Tested on 19 Feb., 1982	62
23. Strain Versus Load at Base, Line H, Shell No.1, Tested on 19 Feb., 1982	63

**THIS BOOK
CONTAINS
NUMEROUS PAGES
WITH THE ORIGINAL
PRINTING BEING
SKEWED
DIFFERENTLY FROM
THE TOP OF THE
PAGE TO THE
BOTTOM.**

**THIS IS AS RECEIVED
FROM THE
CUSTOMER.**

List of Figures (Continued)

Figure	Page
24. Strain Versus Load at The Patched Region Between Lines G and H, Tested on 19 Feb., 1982	64
25. Measured and Theoretical Loads on Column, Shell No.1, Tested on 19 Feb., 1982	65
26. Deflection Profiles for Lines A and B of Shell No.1, Tested in Jan.-Feb., 1982	66
27. Deflection Profiles for Lines C and D of Shell No.1, Tested in Jan.-Feb., 1982	67
28. Deflection Profiles for Lines E and F of Shell No.1, Tested in Jan.-Feb., 1982	68
29. Deflection Profile for Line F of Shell No.1, Tested on Feb. 19, 1982	69
30. Deflection Profile for Line G of Shell No.1, Tested in Jan.-Feb., 1982	70
31. Deflection Profile for Line H of Shell No.1, Tested in Jan.-Feb., 1982	71
32. Deflection Profile for Line I of Shell No.1, Tested in Jan.-Feb., 1982	72
33. Deflection Profile for Line J of Shell No.1, Tested in Jan.-Feb., 1982	73
34. Deflection Profiles for Lines K and L of Shell No.1, Tested in Jan.-Feb., 1982	74
35. Deflection Profile for Level No.1 of Shell No.1 at 2.8 Psi (19.3 KPa), Tested in Jan.-Feb., 1982 ...	75

List of Figures (Continued)

Figure	Page
36. Deflection Profile for Level No.2 of Shell No.1 at 2.8 Psi (19.3 KPa), Tested in Jan.-Feb., 1982 ...	76
37. Deflection Profile for Level No.3 of Shell No.1 at 2.8 Psi (19.3 KPa), Tested in Jan.-Feb., 1982 ...	77
38. Deflection Profile for Level No.4 (Throat) of Shell No.1 at 2.8 Psi (19.3 KPa), Tested in Jan.-Feb., 1982	78
39. Deflection Profile for Level No.5 of Shell No.1 at 2.8 Psi (19.3 KPa), Tested in Jan.-Feb., 1982 ...	79
40. Deflection Profile for Level No.6 of Shell No.1 at 2.8 Psi (19.3 KPa), Tested in Jan.-Feb., 1982 ...	80
41. Deflection Profile for Level No.7 of Shell No.1 at 2.8 Psi (19.3 KPa), Tested in Jan.-Feb., 1982 ...	81
42. Deflection Profile for Level No.8 of Shell No.1 at 2.8 Psi (19.3 KPa), Tested in Jan.-Feb., 1982 ...	82
43. Deflection Profile for Level No.9 of Shell No.1 at 2.8 Psi (19.3 KPa), Tested in Jan.-Feb., 1982 ...	83
44. Deflection Profile for Level No.10 of Shell No.1 at 2.8 Psi (19.3 KPa), Tested in Jan.-Feb., 1982 ...	84
45. Deflection Profile for Level No.11 of Shell No.1 at 2.8 Psi (19.3 KPa), Tested in Jan.-Feb., 1982 ...	85
46. Failed Region from Outside, Shell No.1, Test No.2 ..	86
47. Failed Region from Inside, Shell No.1, Test No.2 ...	87
48. Outside View of Hole, Shell No.1, Test No.2	88
49. Inside View of Hole, Shell No.1, Test No.2	89

SYNOPSIS

In the past ten years the use of natural-draft cooling towers in Europe and North America has increased. These hyperboloids of revolution have increased in size from 115 ft. (35 m) in 1914 to 495 ft. (151 m) in 1979 with 656 ft. (200 m) contemplated for the near future.

Following the catastrophic collapse of three of the eight towers in Ferrybridge, England, in 1965 (5), an intensified research was initiated to understand the behavior of this type of shell and to find answers to these spectacular structural failures. Further interest and need for more and better understanding of the structural behavior of hyperbolic natural-draft cooling towers became urgent after the failure of the cooling tower in 1973 at Ardeer, Scotland, some eight years after construction. This structural tragedy at Ardeer inspired research in the effects of geometry imperfections in cooling towers especially. Most of the experimental work has been on small elastic models and very little information is available on the results of physical testing of concrete models. Consequently, there appears to be a gap between theoretical and true behavior of these giant concrete structures.

The work described herein, is on the testing procedure, behavior, and effects of imperfections on the response of a reinforced concrete cooling tower model subjected to axisymmetric loading (vacuum).

The shell is nominally 0.5 in. (13 mm) thick, 12 ft. (3.65 m) high, and 9.33 ft. (2.84 m), 6 ft. (1.82 m), and 6.45 ft. (1.96 m) in diameter at the base, throat, and top, respectively.

CHAPTER I

INTRODUCTION

Hyperbolic, natural-draft cooling towers are probably the largest reinforced concrete thin-shell structures being built today. Because of the growing need for electric power in the industrialized societies, the use of taller and larger cooling towers with higher cooling capacities has become continually necessary to dissipate large quantities of heat in power stations. Since 1914 the size of these towers has increased from 115 ft. (35 m) to 495 ft. (151 m) in 1979 and towers as high as 656 ft. (200 m) are being considered for the near future.

The basic reason for using the hyperbolic shape for cooling towers is that it is highly efficient in producing a natural draft of air compared to the cylindrical or conical shapes. Besides, the hyperbolic shape provides much greater structural strength due to the double curvature of the shell.

The principal function of a cooling tower is to cool and reuse large quantities of water. The general operational system can be summarized as follows: hot water is pumped to a certain height and then through a piping system it reaches nozzels which splash it over a system called filling or stacking. the function of the filling or stacking is to scatter the water into films or droplets which will provide a larger surface area for the cooling air and hot water to contact. The air, which enters into the base of the tower, is forced upward by

atmospheric pressure difference or the so-called chimney effect. The rising air passes through the droplets or films of hot water and cools them by evaporation and convection. The cooled water is then collected in a pond at the bottom of the tower and is ready to be returned into the condenser system for use.

Even though natural-draft cooling towers consist of several structural units, the shell part (hyperboloid of revolution) remains in the center of attention and demands most of the work and analysis in design and construction.

As a result, and due to collapse of three cooling towers at Ferrybridge, England, and one at Ardeer, Scotland, researchers have become more concerned about the true behavior of these giant reinforced concrete structures. Unfortunately, most of the work is analytical and very few buckling experiments have been carried out on concrete or micro-concrete models subject to axisymmetric or asymmetric loads. Even the experimental results available are mostly for metal or plastic models.

The experiment reported here is on a simple, non-offset, and repaired micro-concrete hyperboloid of revolution. The goals of this study are to obtain some experimental evidence on the buckling behavior of this type of concrete shell and the effects of geometry imperfections under axisymmetric pressure (vacuum).

CHAPTER II

REVIEW OF LITERATURE

Although hyperbolic natural-draft cooling towers are probably the largest reinforced thin-shell structures being built today, there has been very little experimental research on the behavior and stability of this type of shell (2). Perhaps, the most extensive experimental study of model cooling towers has been carried out by Der and Fidler (13). Their electroformed copper and PVC (Polyvinyl Chloride) models were subjected to wind loading in a compressed air tunnel. All the models failed by a snap-through of the upper rim with little noticeable progressive deflection prior to buckling.

In Reference 4, Billington and Harris review tests used to investigate the buckling of roof shells and shell walls. They categorize hyperbolic cooling towers as shell walls where the primary loads causing buckling are horizontal and transient (wind or seismic).

Even though, wind loadings are the governing design criteria for hyperbolic natural-draft cooling towers, there seems to be a lack of experimental evidence regarding the stability of concrete shells for this type of loadings. Most of the pertinent tests of this nature have been conducted on plastic or metal models (13). Nevertheless, Abel and Gould in their paper (2) identify three methods for the stability analysis of large concrete hyperboloids subject to wind

loadings based on axisymmetry (15,29). In References 14 and 15, Ewing gives a complete analytical treatment of cooling tower stability. He uses a linearized theory to analyze hyperboloids of constant thickness without stiffening rings or flexible supports both under axisymmetric pressures and non-axisymmetric wind loads. His conclusion is that the theoretical axisymmetric buckling pressures are smaller than the peak wind pressure associated with bifurcation of the same hyperboloid. Langhaar and Miller (22) also reached the same conclusion for fixed-free cylinders subjected to both axisymmetric and asymmetric radial pressures.

Veronda and Weingarten (33) have written computer programs for linear buckling and linear and nonlinear prebuckling analysis of hyperboloidal shells using the finite element method. Cole, Abel, and Billington (7,8) have also developed a finite-element computer program to study the problems encountered in design when considering stability. In Reference 8 the authors describe in their work those parameters which are characteristic of actual cooling towers to estimate the bifurcation buckling loads.

However, it should be mentioned that neither of the three methods given in Reference 2 has been accepted or used universally by designers and researchers who differ on such matters as local buckling versus global stability treatment, bifurcation analyses versus limit-point analyses, reduced shell theories versus full shell theories, and axisymmetric analyses versus non-axisymmetric analyses.

Be that as it may, Abel and Gould (2) say that for routine design purposes bifurcation calculations with approximate methods based on axisymmetry can supply reasonable estimates for buckling pressure of hyperboloids subject to wind loading.

In two recent studies (19,23), a reinforced concrete cooling tower built in Port Gibson, Miss., USA subjected to wind loading is investigated in detail. The investigators believe that failure of a reinforced concrete cooling tower would not be initiated by buckling but rather by rapid propagation of cracks in the tensile zone followed by temporary stiffening and, finally, by yielding of the reinforcement. For that matter, the tensile strength of concrete is considered to be of critical importance in the safety of the shell against collapse. In Reference 23, Mang, et al., conclude that results based on an equivalent axisymmetric pressure are on the unsafe side of corresponding results for the actual wind load. It is also believed in both studies that linear-elastic non-axisymmetric analysis is an appropriate tool for the design of cooling towers subject to wind loads.

Since the collapse of the 350 ft. high Ardeer cooling tower in Scotland, more research and study has been conducted in order to gain better knowledge of the effects of imperfections in the geometry of reinforced concrete cooling towers.

In Reference 11, Croll, Kaleli, and Kemp analyze a cooling tower model with axisymmetric geometry imperfections represented as a series of piecewise continuous second-order

rotationally symmetric shells of the same general form as that of the perfect shell. Their analysis yields hoop forces due to imperfections and meridional bending moments. This analysis is based on the assumption that flexural failure due to the imperfection generated meridional moments will not precipitate collapse, but that the shell has sufficient ductility to enable a redistribution from bending to membrane action to occur. It is also stated that variations in the elevation of the imperfection are found to have a significant influence on the stress changes.

Croll and Kemp have two approaches to examine changes in hoop tensions that occur in an axisymmetric meridionally imperfect shell. The first approach (10) is the same as that given in Reference 11 and a finite difference discretisation is used to solve the appropriate equations for shell bending. In the second approach (12), however, a normal pressure distribution is chosen to simulate the geometric imperfection so that it is statically equivalent to the out-of-balance forces that would be present when it is considered that the membrane stresses of the perfect shell act on the geometrically imperfect shell.

Mungan (26) tested several shell models made of a cold epoxy resin and hardner to determine the primary buckling stresses of nearly perfect hyperboloidal-type shells and he concluded that buckling depends primarily on the local imperfections, wall thickness, and the stress state acting in

the model. He also reached the conclusion that buckling is always initiated at a point with an imperfection resulting from a reduced thickness. Mungan in a later study (25) shows that the buckling behavior of shells can be improved by placing stiffening rings in the models.

In a recent paper (24) Mungan states that model tests showed that buckling always began locally. According to him cooling tower shells buckle locally in presence of even slight imperfections and the influence of initial imperfections is more than the influence of boundary conditions on local buckling. He emphasizes that in the buckling design of reinforced concrete cooling tower shells local buckling has to be prevented everywhere within a certain safety margin in order to fulfill global or overall stability of the shell. This is the idea behind what he calls the Buckling Stress States (BSS) approach developed by him.

The preceding approach, which is recommended by the International Association for Shell and Spatial Structures (IASS), is criticized by Abel, et al. (1). They question the applicability of the approach to actual cooling tower design and list three problems associated with it: (1) factoring of boundary-condition sensitivity into the approach in an uncertain way; (2) lacking a way to include the important influence of concrete cracking; and (3) applying a safety factor of five to both wind and dead load and in turn creating an unrealistic stress condition.

Gupta and Al-Dabbagh have also studied the effects of meridional imperfections in cooling towers. In Reference 3 they assume that the meridional shape of imperfection is a combination of two straight lines. Later Gupta, et al. (18) assumed a general shape which would have the straight line or circular configuration as two extremes.

Furthermore, they state that: (a) hoop stresses are increased as a result of imperfections; (b) meridional moment plays an important role in the safety of the tower; and (c) imperfection stresses should be considered in the design of cooling towers.

On the other hand, there are those who believe that shells of negative Gaussian curvature, hyperboloids of revolution, under axisymmetric loadings are not significantly sensitive to geometric imperfections (21,33).

In Reference 6, the results of the first test of the shell under consideration here are discussed. The failure is reported to be similar to that of a spherical concrete shell. The author states that this type of failure has never been reported for hyperbolic shells before. The geometry and thickness imperfections are considered to have produced additional stresses and moments. The author also states that the structure responded unsymmetrically and the failure mode was initiated by some mechanism other than by exceeding material limits.

Yet there is no clear and full understanding of the behavior of cooling towers in the real world. Consequently,

more research and effort should be directed in this area considering the effects of such factors as the true shell geometry, realistic support conditions, gravity and thermal loadings, orthotropic materials, and variations of wind pressure.

CHAPTER III

SHELL TEST ARRANGEMENTS

The shell under consideration here has been designed, erected, and tested once previously. The model is 12 ft. (3.65 m) high with throat radius of 36 in. (0.91 m), base radius of 56 in. (1.42 m), and nominal thickness of 0.5 in. (13 mm). The uniform thickness of 0.5 in. was not however accomplished very accurately during construction and various thicknesses were recorded which will be looked at later. Fig. 1 shows the geometry of the shell in more detail.

In References 6,16,30, a complete, detailed, and pictorial description of design and construction of support facilities, assembling of reinforcing wires, form work, model materials, and construction sequence of the shell model is given. The results of the first buckling test are also discussed in Reference 6.

The hole which occurred in the shell as a result of the first experimental test (6) was patched up and later strain gages were mounted on the inside and outside of this patched region. The properties of the patching mix and reinforcing steel are given in Table 1. Table 2 displays the results of the cylinder tests.

STRAIN AND DISPLACEMENT INSTRUMENTATION

Temperature compensated electrical resistance foil strain

gages were used. These were two element rectangular rosettes with a gage length of 0.125 in. (3.18 mm). The gages were positioned to be parallel to the circumferential direction (even-numbered gages) and meridional direction (odd-numbered gages).

Dial gages mounted on a portable beam (6), which could be moved to various circumferential locations, were used to record deflection measurements. These had a least reading of 0.001 in. (0.0254 mm) and travel of 2 in. (50 mm).

Locations for strain, deflection, geometry, and thickness measurements are shown in Fig. 2 and 3. More information on these items can be found in References 6, 16, and 17.

LOADING EQUIPMENT AND TESTING PROCEDURE

The loading equipment essentially consisted of a high vacuum, high capacity pump and three or four lower capacity accessory pumps; lines and fittings; and a mercury manometer. The high capacity pump had a shut off valve which permitted a constant pressure (vacuum) to be maintained.

The testing procedure was:

1. Initialize strain and dial gage data;
2. Apply load to desired level and maintain;
3. Record strain data and dial data;
4. Repeat steps 2 and 3 until the final load level;
5. Move the portable beam to the next location and repeat steps 1-4.

The main difficulty encountered during testing was the leakage of air from the top and bottom cover plates. Hence, more bracing was fastened to the plates to decrease their movement due to suction. The joints and connections were also sealed with different commercial compounds (silicon rubber, liquid nail, resin) where silicon rubber proved the most efficient and air-tight.

CHAPTER IV
TEST RESULTS AND ANALYSIS

SHELL GEOMETRY

After the first testing of the shell (6), measurements of deviation from ideal geometry were taken at 132 locations. The deviation values shown in Table 3 represent the differences from the ideal shell horizontal radius to the outer surface at the locations indicated in Figs. 2 and 3.

It is attempted here to improve the deviation data by considering the actual thickness values given in Reference 6 and shown in Table 4. Sample calculations are given in Appendix C for two throat locations with geometrical description shown in Fig. 4. Table 5 gives the complete list of the improved data of deviation from ideal mid-surface geometry with the maximum deviations in the radii being +3.2%, -2.7%.

The percent deviation in a vertical distance along a meridian expressed as the slope S is found from:

$$S = (2\Delta/H)100$$

where

$$\Delta = \Delta r_{ij} - 1/2 (\Delta r_{i-1,j} + \Delta r_{i+1,j})$$

$$H = \text{gage length of 24 in. (60.96 cm)}$$

Δr_{ij} = center line radial deviation at the center of the vertical gage length

$\Delta r_{i-1,j}, \Delta r_{i+1,j}$ = center line radial deviation at the ends of the vertical gage length

i = gage number from 1-11

j = line number from A-L, i.e., from 1-12

The maximum values of S for each vertical line are also presented in Table 5. The overall maximum values of S are about + 2.65%.

The data in Table 5 is used to plot circumferential deviation profiles from ideal shell middle surface geometry at all eleven dial gage locations, Figs. 5-15. These display the out-of-roundness of the shell. Notice that they generally follow the same oval pattern.

Hence, the geometry of the model shell is not as accurate as encountered in practice today. Notwithstanding, as geometrical scale becomes smaller (a scale factor of 30 for this model), the chance of achieving corresponding tolerances becomes smaller too, if the model is to represent the prototype.

SHELL THICKNESS

As mentioned previously the shell varied widely in thickness particularly in the first lift (locations of the three lifts are shown in Fig. 2). The reason for this included lack of experience and difficulties encountered during casting of the shell, e.g., form bulging and separation, etc. (6).

In order to have a better picture of the thickness variation, a thickness contour map of the shell is shown in Fig. 16 with contour intervals of 0.1 in. (2.54 mm). It can be seen from the map that lift one shows great thickness variation

while lifts 2 and 3 show less variation and better uniformity. The percent deviation from mean values of thickness at each elevation for lifts 2 and 3 are given in Table 6. It is observed that the largest deviations from the mean are +82% and -60%. Corresponding deviations for Mungan's large plastic models (26) are +26% and -22% as given in Table 7. Thickness deviations on a concrete model of a cylindrical shell reported by Harris, et al. (28) are +46%, -24%.

Geometry and thickness imperfections produce additional forces and moments which will be discussed later.

STRUCTURAL RESPONSE AND FAILURE

After a long and cumbersome buckling test the shell finally failed at a pressure (vacuum) of 3.7 Psi (25.53 KPa). This is about 20% greater than the pressure of 3.1 Psi (21.4 KPa) that caused failure in the first test (6). The load that commenced failure is slightly more than half that predicted using the method of Reference 17. The method of Reference 20 using a grid analogy and considering linear material response gave a buckling load of 3.2 Psi (22 KPa).

Strain versus load curves up to the failure load of 3.7 Psi (25.53 KPa) are presented in Figs. 17-24. The overall response is linear and no indication of buckling is observed. Fig. 24 shows the curves for the patched region which is the failure region of the first test. These plots do not show any sudden jump of the strain and are generally linear up to the failure pressure. Also shown in the figures are the theoretical

curves based on membrane theory amended by meridional imperfection. These are plotted using the following equations:

$$\epsilon_{\theta} = (N_{\theta} - \mu N_{\phi}) / t E_c$$

$$\epsilon_{\phi} = (N_{\phi} - \mu N_{\theta}) / t E_c$$

where

Poisson's ratio, μ , and Young's modulus of concrete, E_c , are 0.16 and 3.62×10^6 Psi (24.9 GPa), respectively (6).

In calculating the membrane forces N_{ϕ} and N_{θ} it was assumed that the shell carried 5/9 of the load from the top plate (16). In addition the method given by Gupta and Al-Dabbagh (18) was followed in order to include the effects of measured surface geometry imperfections which caused additional hoop force and meridional bending moment. This process is demonstrated in Appendix C through sample calculations at the throat on vertical line H.

The load-strain curves show good agreement between average (membrane) values and theoretical values. For example, at 4 ft. (1.22 m) below the throat, Fig. 22, the deviation between the average and theoretical curves becomes very small while at the base, Fig. 23, this deviation is almost zero.

Evidently the structural failure did not initiate by exceeding material limits because the maximum negative strain recorded -169×10^{-6} in./in., Fig. 21-- is equivalent to a concrete compressive stress of about 690 Psi (4.76 MPa).

Values of the experimental forces and bending moments at the locations of the strain gages, including the patched region, are given in Table 8 for the failure load of 3.7 Psi (25.53 KPa). The equations and sample calculations for computing these forces and moments are presented in Appendix C. From Table 8 it can be observed that,

1. The patched region does not have the largest forces and moments.
2. The forces at the three throat locations (90 degree apart circumferentially) are not equal; hence the structural response is unsymmetrical.
3. At all locations except that just below the top ring N_{θ} predominates.
4. At the base and top of the shell M_{θ} and M_{ϕ} are significant, respectively.

Figure 25 displays the experimental and theoretical plots for the compressive support column loads. The curves are plotted from the equations:

$$\text{Experimental, } P = 1/2 (\epsilon_{c_1} + \epsilon_{c_2}) E_s A$$

$$\text{Theoretical, } P = 4/9 \pi r^2 q$$

In which,

ϵ_{c_1} and ϵ_{c_2} are the recorded strains for the column;

E_s is the modulus of elasticity of steel, 29×10^6 Psi (200 GPa);

A is the cross sectional area of the column given in Table 1;

r is the radius of the top plate;

In plotting the theoretical curve it was assumed that the column carried $4/9$ of the top cover load (16).

Deflection profiles along the twelve meridional lines, A-L, are displayed in Figs. 26-34. Local perturbations can be noticed on lines B, E, and L which might suggest development of cracks or failure on or close to these lines. However, neither cracks nor failure occurred at these locations. The failure location of the first buckling test (patched region) appears to act as an inflection point because line G has outward displacement while line H moved inward. Deflection in the region of the hole seems to be the largest along line J. Also the direction of of the deflection curve is the same as the failure - inward. The two deflection profiles for line F --Figs. 28 and 29-- are for loads of 2.8 Psi (19.3 KPa) and 3.7 Psi (25.53 KPa), respectively. Notice that Fig. 29 is plotted up to the failure pressure of 3.7 Psi. Although the data for the two plots were taken at different times the resemblance is very good.

The circumferential plots of the displacements for all eleven dial gage locations are presented in Figs. 35-45 for a load of 2.8 Psi (19.3 KPa). This same oval pattern was obtained for virtually all of the load stages. This deflection pattern is not associated with buckling but is probably caused by the